J. Fluid Mech. (1996), *vol.* 318, *pp.* 1–29

Unsteady counterflowing strained diffusion flames: diffusion-limited frequency response

By FOKION N. EGOLFOPOULOS AND CHARLES S. CAMPBELL

Department of Mechanical Engineering, University of Southern California, Los Angeles, CA 90089-1453, USA

(Received 11 August 1994 and in revised form 3 November 1995)

A detailed numerical study has been conducted on the effect of unsteadiness on the dynamics of counterflowing strained diffusion methane/oxygen/nitrogen flames. The modelling included the solution of the unsteady conservation equations of mass, momentum, energy, and species along the stagnation streamline in an opposed jet using detailed descriptions of chemistry and transport. The unsteadiness was introduced by independently imposing sinusoidal variations of the reactant velocity, concentration and temperature at the exits of the nozzles. The results demonstrate that the flame's response is quasi-steady at low frequencies, while at higher frequencies the amplitudes of the induced oscillations are reduced and phase shifted with respect to the imposed signal. At still higher frequencies, the flame no longer responds to the oscillations in the external field. A rigorous physical explanation of the frequency response was provided from first principles by identifying that oscillations imposed at the nozzle exits result in reactant concentration and temperature oscillations at the outer edge of the preflame diffusive zones. The diffusion attenuates the oscillations in this zone in a manner analogous to the velocity attenuation in Stokes' second problem. The validity of the analogy was confirmed by examining flames over a wide range of frequencies and initial conditions. The current analysis also provided a criterion for the cutoff frequency separating the quasi-steady and transient regimes – information which can be useful in the establishment of laminar flamelet libraries.

1. Introduction

Fundamental understanding of the structure and dynamic response of laminar flamelets is expected to significantly contribute towards the better understanding of turbulent combustion (e.g. Libby & Williams 1982, 1984; Peters 1984, 1986; Law 1988). Whether turbulent combustion takes place in the laminar flamelet regime depends on the relative magnitude of the flame thickness, l_f, and the smallest turbulent mixing scale, such as the Kolmogorov scale l_k (Peters 1986). If l_f is smaller than l_k, then the flame retains its laminar-like structure which can be corrugated and/or wrinkled. Each segment of the reacting front can be treated as a laminar flamelet which is subjected to various amounts of aerodynamic stretching by the adjacent vortices (Peters 1986). There is evidence (Bracco 1988), that such conditions exist in internal combustion engines, making the laminar flamelet concept a promising one. This has, therefore, been the motivation for extensive theoretical and experimental studies on the dynamics of *steady* strained laminar flames (e.g. Libby & Williams 1982, 1984; Miller *et al.* 1984; Peters 1984, 1986; Wu & Law 1984; Williams 1985; Smooke, Puri & Seshadri 1986; Kee *et al.* 1988; Law 1988; Zhu, Egolfopoulos & Law 1988; Rogg 1989;

Chelliah *et al.* 1990; Dixon-Lewis 1990) and significant insight has been gained into the coupling between the aerodynamic stretching and the elementary processes of molecular transport and chemical kinetics.

In reality however, if burning occurs in the flamelet regime, the combustion will take place in highly unsteady environments, resulting not only from fluctuations of the local velocity and consequently the strain rate, but also from fluctuations of the incoming reactant concentrations and temperatures. In a turbulent flow field, while the large-scale eddies establish the magnitude of the mean strain rate, fluctuations around this mean value can be caused by smaller eddies with characteristic turnover times which are comparable to the characteristic diffusion time for sufficiently large turbulent Reynolds numbers (Im & Law 1993; Im *et al.* 1995). Furthermore, the random and intense fluctuations of the turbulent flow field can lead to the mixing of unburned cold reactants with hot reaction products and thus lead to local oscillations of reactant concentration and temperature. The importance of the understanding of the transient response of flames has been recognized in early studies (Strahle 1965; Clarke & Stegen 1968; Carrier, Fendell & Marble 1975; Linan & Crespo 1976; Saitoh & Otsuka 1976; Spalding 1978) and more recently (Haworth *et al.* 1988; Rutland & Ferziger 1990; Stahl & Warnatz, 1991; Cetegen & Bogue 1991; Cetegen & Pines 1992; Darabiha 1992; Ghoniem *et al.* 1992; McIntosh, Batley & Bridley 1993; Im & Law 1993; Kim & Williams 1994; Im *et al.* 1995). Such unsteady investigations are limited in number compared to their steady counterparts.

The introduction of unsteadiness in combustion is a challenge since its characteristic timescales can couple with the timescales of convection, diffusion, and reaction. A major concern is whether and to what extent the rich knowledge of steady combustion is applicable to unsteady situations and it is highly desirable, especially in the modelling of turbulent combustion, to be able to decide whether transient effects will be important on a flamelet, given the local conditions of turbulence. Therefore, it is important to formulate criteria which will provide estimates of the boundary between the quasi-steady and transient responses.

While these previous studies on unsteady combustion have provided qualitative insight into the flamelet response to unsteadiness, a quantitative criterion allowing for the distinction between the quasi-steady and transient regimes has not been formulated and explained from first principles. Ideally, such a distinction could be obtained by systematically exposing laminar flames to far-field harmonic unsteadiness and by allowing the frequencies to vary from very low to very high values. The case of harmonically varying strain rate is also of particular interest to turbulent combustion since the wide range of eddy lengthscales can lead to a wide range of characteristic frequencies. Therefore, the understanding of the complete frequency response of the flame is essential.

This approach has been taken in a limited number of studies (Strahle 1965; Saitoh & Otsuka 1976; Stahl & Warnatz 1991; Cetegen & Bogue 1991; Cetegen & Pines 1992; Darabiha 1992; Ghoniem *et al.* 1992; Im & Law 1993; Im *et al.* 1995). The early analytical work of Strahle (1965) on convective droplet burning at a stagnation point when a small-amplitude sound wave was introduced into the free stream, has shown that the burning rate appears to have a reduced response at high frequencies compared to the low frequencies. More relevant to the current study, Saitoh & Otsuka (1976) conducted a combined analytical and experimental study for unsteady counterflow flames and in both theory and experiments the high-frequency attenuation was observed. Stahl & Warnatz (1991) made much the same observations using a numerical study of unsteady strained premixed flames which employed detailed descriptions of

molecular transport and chemical kinetics. Darabiha (1992) also performed a detailed numerical study and observed that the cutoff frequency between quasi-steady and transient response becomes larger for higher fuel mass fraction in the fuel stream (which also makes the burning rate stronger). Cetegen & Bogue (1991), Cetegen & Pines (1992), and Ghoniem *et al.* (1992) have all made similar observations based on numerical studies of unsteady strained diffusion flames by using a one-step description of the chemical kinetics. In none of the studies, however, was a physical explanation provided and no criterion was developed appropriate to quantify the transition frequencies between the quasi-steady and transient regimes. The analytical work of Im & Law (1993) and Im *et al.* (1995) on unsteady counterflow diffusion flames using large-activation-energy asymptotic analysis, showed a similar frequency response to all other studies and a limited physical explanation was provided. Here, the quasi-steady response was attributed to the fact that at low frequencies the characteristic oscillation time is much longer than the diffusion time in the flame structure so that the flame response is quasi-steady. The failure of the flame to respond at high frequencies was attributed to the phase lag which develops between the 'strain rate variation and the response of the flame sheet'. But while this argument explains the phase lag, there is no clear connection between that phase lag and the attenuation of the flame response at high frequencies.

The verification of theoretical results on unsteady flames will involve complex experiments and it is important that guidelines are provided from relevant analysis. The configuration which offers the most flexibility for the study of strained flames is the opposed-jet counterflow which has been extensively used for steady studies (e.g. Libby & Williams 1982, 1984; Miller *et al.* 1984; Wu & Law 1984; Smooke *et al.* 1986; Yu, Law & Wu 1986; Kee *et al.* 1988; Law 1988; Zhu *et al.* 1988; Rogg 1989; Chelliah *et al.* 1990; Dixon-Lewis 1990). In their detailed numerical simulations, Stahl & Warnatz (1991) and Darabiha (1992) have assumed potential flow originating at infinity, which is not a good representation of the experimental counterflow flow field (Kee *et al.* 1988; Chelliah *et al.* 1990) in which the flow originates from two opposed nozzles separated by a finite distance.

In view of the above considerations the present investigation had two main goals. First, to numerically simulate unsteady opposed-jet counterflowing methane/oxygen/nitrogen diffusion flames in a finite domain (i.e. issuing from finite-sized nozzles located at finite distances from the flame) by using detailed description of the chemistry and molecular transport, and to quantify the response of the flame to the variations in the free-stream reactant properties. Secondly, to provide enhanced insight into the elementary physico-chemical mechanisms which control the flame's frequency response and scaling laws from first principles.

Diffusion flames were chosen to be studied first as, for conditions which are not near extinction, the diffusion processes control the overall burning, indicating a possible coupling between the unsteadiness and the diffusion processes. Furthermore, reactant leakage and heat loss to both sides of the flame make diffusion flames very sensitive to straining and, therefore, can profoundly affect their structure. Methane was chosen because it is a practical fuel with well understood kinetics, and has not previously been used in unsteady diffusion flames calculations. The diffusion flames chosen to be studied herein are characterized by large Damköhler numbers, defined as the ratio of a characteristic convective time to a characteristic chemical time, which implies that the actual reaction zones are very thin. This ensures the relevance of the study to the concept of laminar flamelets in turbulent non-premixed combustion.

Finally, it should be noted that although physical insight can be obtained by solving

the problem using one-step chemistry, the use of detailed modelling is a significant advancement of the analysis, since all the elementary processes of molecular transport and chemical kinetics are described with the minimum number of assumptions. This leads to a more accurate determination of the flame's dynamic response, which then can be compared with experiments. Furthermore, such an approach is the only way to capture the details of extinction and intermediate-species (including pollutants) concentrations as functions of the mixture initial conditions and the imposed unsteadiness.

2. Numerical methodology

The numerical simulation of the counterflow was conducted by solving the unsteady conservation equations of mass, momentum, energy, and species concentrations along the stagnation streamline, following the original quasi-one-dimensional formulation of Kee *et al.* (1988) and Dixon-Lewis (1990):

$$\frac{\partial \rho}{\partial t}+2\rho G+\frac{\partial(\rho u)}{\partial x}=0 \qquad \text{(mass conservation)},$$

$$\rho\frac{\partial G}{\partial t}+\rho u\frac{\partial G}{\partial x}+\rho G^2+J-\frac{\partial}{\partial x}\left(\mu\frac{\partial G}{\partial x}\right)=0 \qquad \text{(momentum conservation)},$$

$$\rho\frac{\partial T}{\partial t}+\rho u\frac{\partial T}{\partial x}-\frac{1}{c_p}\frac{\partial}{\partial x}\left(\lambda\frac{\partial T}{\partial x}\right)-\frac{\partial P}{\partial t}+\frac{\rho}{c_0}\sum_{k=1}^{K}Y_k c_{pk} V_k\frac{\partial T}{\partial x}+\frac{1}{c_p}\sum_{k=1}^{K}h_k\omega_k=0 \qquad \text{(energy conservation)},$$

$$\rho\frac{\partial Y_k}{\partial t}+\rho u\frac{\partial Y_k}{\partial x}+\frac{\partial}{\partial x}(\rho Y_k V_k)-W_k\omega_k=0 \qquad \text{(species conservation)},$$

with

$$G\equiv\frac{\partial v}{\partial r}=\frac{v}{r}=G(x) \quad \text{and} \quad J\equiv\frac{1}{r}\frac{\partial P}{\partial r}.$$

In the above equations ρ is the density, P is the pressure, μ is the mixture viscosity, λ is the mixture conductivity, c_p is the mixture specific heat, c_{pk} is the specific heat of species k, h_k is the molar specific enthalpy of species k, ω_k is the molar production rate of species k, W_k is the molecular weight of species k, Y_k is the mass fraction of species k, u is the axial convective velocity component, v is the radial convective velocity component, K is the total number of species, and V_k is the mass diffusion velocity of species k. All the details regarding the derivation and assumptions of the above equations are described in Kee *et al.* (1988) and Dixon-Lewis (1990).

The solutions were obtained in a finite domain configuration in order to simulate actual experiments such as that schematically represented in figure 1. However, the results should still be qualitatively similar to the potential flow cases studied by Stahl & Warnatz (1991) and Darabiha (1992). It should be also noted that the present quasi-one-dimensional formulation aims to simulate only the region around the stagnation streamline and that other finite domain effects might appear in a full axisymmetric analysis. Unlike previous studies (Stahl & Warnatz 1991; Darabiha 1992; Ghoniem *et al.* 1992), the strain rate in the present investigation is not explicitly specified, but instead is a consequence of the imposition of unsteady velocity fields in a stagnation

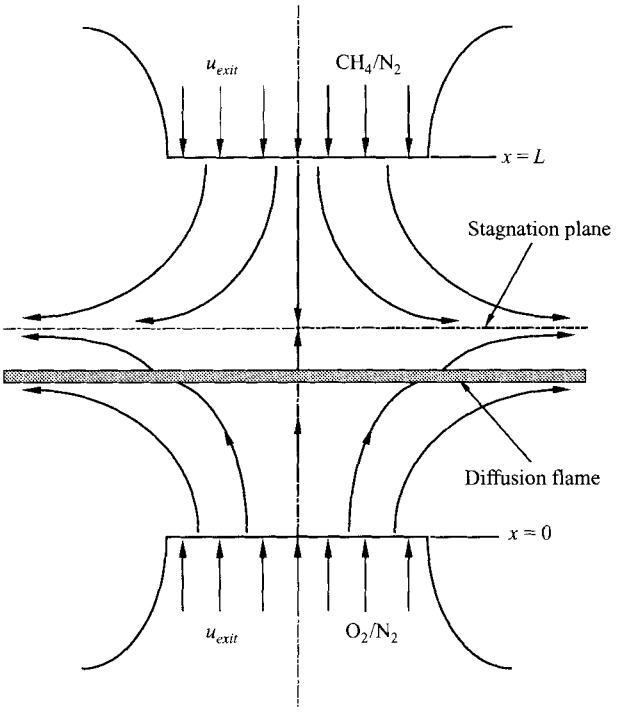

FIGURE 1. Schematic of the counterflow.

flow configuration; as straining in a turbulent environment results from flow-field non-uniformities, this is probably more representative of the behaviour in actual turbulent flows. It was also assumed that the gases as they leave the nozzle exhibit no radial variations in velocity, temperature, and concentration. As a consequence, the whole flow field is characterized by a uniform radial pressure curvature J which is an eigenvalue of the problem (Kee *et al.* 1988; Dixon-Lewis 1990; Stahl & Warnatz 1991). Furthermore, it was assumed that no vortex rings or other instabilities develop as the properties oscillate.

In the present study the spatially varying pressure that drives the convection appears only in the momentum equation. As the system is assumed to exhaust into an infinite domain at a constant pressure (here 1 atm.) any spatio–temporal pressure variations are assumed to be small perturbations and not to noticeably couple with the thermodynamic and transport properties and the reaction rates. Similarly, the $\partial P/\partial t$ term in the energy equation has been neglected. In general, far-field velocity oscillations can lead to both pressure and velocity effects (Strahle 1965; McIntosh *et al.* 1993; Im & Law 1993; Kim & Williams 1994; Im *et al.* 1995) but for characteristic frequencies of the imposed disturbances well below the acoustic regime (Kim & Williams 1994) and for open flames, the velocity effect can be considered as the dominant one. For studies in closed vessels, however, the pressure variations must be coupled with all properties and the $\partial P/\partial t$ term must be retained in the energy equation. In a future investigation possible coupling of the pressure oscillations with all conservation equations and properties will be investigated.

The diffusion flames studied herein result from the impinging of a fuel stream emerging from the upper nozzle onto an oxidizer stream emerging from the lower nozzle (figure 1). The fuel stream was a mixture of CH_4 and N_2 and the oxidizer stream

a mixture of O_2 and N_2. As plug flow conditions were assumed, the boundary conditions at the exit of the lower ($x = 0$) and upper ($x = L$) nozzle exits are

$$x = 0: \quad Y_{O_2} = Y_{O_2,x=0}, \quad Y_{CH_4} = 0 \qquad Y_{N_2} = Y_{N_2,x=0}, \quad G = 0;$$
$$x = L: \quad Y_{O_2} = 0, \qquad Y_{CH_4} = Y_{CH_4,x=L}, \quad Y_{N_2} = Y_{N_2,x=L}, \quad G = 0.$$

Initially, the problem for a steady flame is solved to provide a base state upon which the subsequent oscillations are imposed. For $t < 0$, the flow is assumed to correspond to that of a steady solution and at $t = 0$, the unsteadiness is introduced in the reactant properties at the exit of the nozzles, H_{exit}; the symbol H is used generically to represent the oscillated quantity be it the reactant velocity, mole fraction, or temperature. In the first realization of this model, it was assumed that the oscillations of H_{exit} had the form

$$H_{exit} = H_{exit,o} + H_{exit,A} \sin(\omega t) = H_{exit,o} + H_{exit,A} \sin(2\pi f t),$$

and was instantaneously imposed on the steady-state solution at $t = 0$. Here, $H_{exit,o}$ is the mean value, $H_{exit,A}$ the amplitude of oscillations, and f and $\omega = 2\pi f$ are the frequency and angular frequency of the oscillations respectively. However, the use of the above equation led to strong numerical oscillations in the initial time steps because of the discontinuity in $\partial H_{exit}/\partial t$ which is zero in the steady solution but becomes instantly non-zero once the external oscillations are imposed. The numerical oscillations of the flame properties were more profound at high frequencies for which the $(\partial H_{exit}/\partial t)_{t=0}$ term can be quite large. To circumvent this, three approaches were used in order to ensure that the gradients $(\partial H_{exit}/\partial t)_{t=0}$ are zero; all three approaches have been tested in the various cases studied herein (and give nearly identical responses). First, the cosine function was used:

$$H_{exit} = H_{exit,o} + H_{exit,A} \cos(\omega t),$$

which ensures $(\partial H_{exit}/\partial t)_{t=0} = 0$. The limitation of this approach is that the initial state must correspond either to the top or the bottom of the cycle and cannot be a steady solution about the mean value. Although not explicitly stated, it appears from his results that this approach was taken by Darabiha (1992). The second approach is to use the sine function with the addition of a damping function $F(t)$ to ensure that $(H_{exit}/\partial t)_{t=0} = 0$ and gradually transitions to a pure sine function within a few time steps. We assumed the form

$$H_{exit} = H_{exit,o} + H_{exit,A} \sin(\omega t) - F(t),$$

where

$$F(t) = \beta t \exp(-\alpha t)$$

and

$$\beta = [H_{exit,A} \sin(\omega \Delta t)]/[\Delta t \exp(-\alpha \Delta t)].$$

Δt is the time step and α a constant of the order of 0.5–1.0. A careful examination of the above formula reveals that $(\partial H_{exit}/\partial t)_{t=0} = 0$ and that the damping effect quickly disappears. For each case, α was chosen to eliminate the damping within 4–5 time steps of the numerical integration, which represents about 1 to 2% of the period of the first oscillation. While this approach is somewhat *ad hoc*, it better approximates the conditions likely to be found in an actual experiment than the sudden imposition of a sine wave. In the third approach the oscillations were initiated by using a cosine function which ensures $(\partial H_{exit}/\partial t)_{t=0} = 0$ and subsequently switches to a regular sine function with the same frequency at a time equal to 0.75 of the first period (when the slopes of the sine and cosine functions match). For flames in which extinction does not occur in the first oscillation period, the above approaches are not crucial, since after

the second period a smooth time response of the flame is established. It was also found that the choice of the approach does not affect the results and scaling laws for vigorously burning flames.

The solution of the equations was obtained by modifying a steady premixed-flame stagnation-flow/half-domain code (Kee *et al.* 1988; Kee 1992, personal communication) and introducing a second-order Crank–Nicolson scheme for the time marching. The code uses finite difference discretization and its expansion to the full domain employed upwind differencing of the convection terms which is somewhat complicated as they have opposite signs on the opposing sides of the stagnation plane. In order to achieve this, a decision-making subroutine was created and used to locate the instantaneous stagnation plane and appropriately discretize the convective terms across it. The code was integrated into the CHEMKIN (Kee, Rupley & Miller 1989) and transport (Kee, Warnatz & Miller 1983) subroutine packages. The kinetic scheme used is an hierarchically developed C_2 mechanism (Egolfopoulos, Du & Law 1992; Egolfopoulos & Law 1994) which satisfactorily predicts the oxidation properties of hydrogen, carbon monoxide, methane, ethane, ethylene, acetylene, and methanol. The simulations were performed on a HP/Apollo 9000/720 workstation.

3. Results and discussion

In all flames studied, the solutions were examined to determine the time variations of the maximum flame temperature, the maximum radical mass fraction, the aerodynamic strain rate, the maximum heat release, the radial pressure curvature eigenvalue, and the instantaneous locations of the flame and the stagnation plane. A typical structure of a strained diffusion flame can be seen in figures 2 and 3. A physical understanding of the flame structure will be essential in understanding the descriptions of the various phenomena described in the subsequent sections.

In figure 2(*a*) it can be seen that the temperature reaches a maximum value, known as the flame temperature and the location of that maximum is taken to be the flame location. For the cases studied herein, the flame is located on the oxidizer side of the stagnation plane. In general, the flame location is determined by the requirement for stoichiometric supply of the reactants; since for this flame the fuel is abundant in the fuel stream and the oxygen is deficient in the oxidizer stream, the flame is preferentially located closer to the oxidizer nozzle. (However, calculations with pure oxygen in the oxidizer stream and reduced concentrations of methane in the fuel stream show that the flame can migrate into the fuel side of the stagnation plane.) As a result, oxygen is supplied to the flame by both convection and diffusion while the fuel is supplied mainly by diffusion. Consequently, as it can be seen in figure 2(*b*), there are behavioural differences between the profiles of fuel and oxygen. While the fuel is completely decomposed before reaching the maximum temperature, the oxygen appears to leak through the flame and penetrate deep into the fuel zone. In figure 2(*a*) it can be also seen that on the oxidizer side, the velocity decreases as the flame is being approached and it reaches a minimum at the location at which the heating effect of the flame becomes important. Then, it rises to a local maximum and eventually decreases towards zero at the stagnation plane. On the fuel side, the velocity simply decreases towards zero at the stagnation plane. Now, for the present study, the imposed aerodynamic strain rate K is defined on the oxidizer side as the gradient of the quasi-linear portion of the velocity profile located just before the local minimum of the velocity (see figure 2*a*); the choice of the oxidizer side for the strain rate determination is more meaningful since the convective velocities of the oxidizer are directly associated

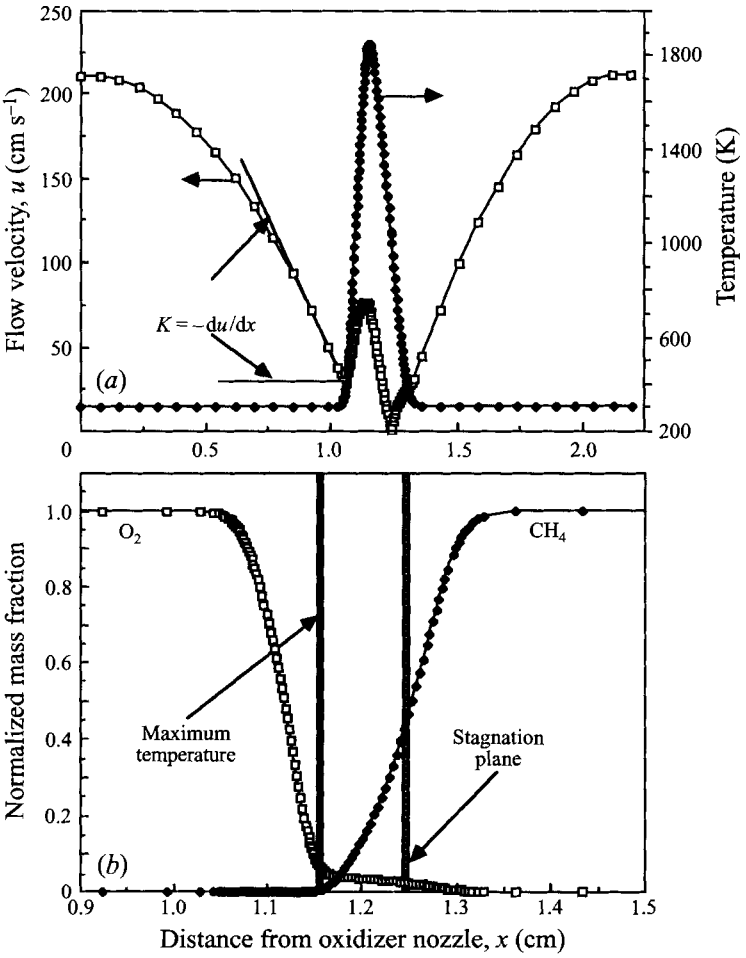

FIGURE 2. Structure of Flame I with $u_{exit} = 210$ cm s^{-1}. Spatial variations of (*a*) flow velocity and temperature, and (*b*) mass fractions of main reactants normalized by their free-stream values.

with the oxygen leakage through the flame that can lead to a drop in flame temperature and eventual extinction. In figure 3(*a*) the profiles of the mass fraction of H radicals Y_H, and the heat release Q, are shown and it is apparent that both attain a global maximum in the vicinity of the maximum flame temperature. Furthermore, the heat release profile has two local maxima, and detailed analysis shows that the smaller is due to the exothermicity of the three-body termination reaction

$$H + O_2 + M = HO_2 + M, \tag{1}$$

which is the main reaction between H and O_2 in this vicinity. The global maximum is due to the exothermicity in the main reaction zone during the CO oxidation. In figure 3(*b*) the mass fraction of O_2 is shown along with the rate of the main branching reaction

$$H + O_2 = OH + O, \tag{2}$$

which is largely responsible for the formation of OH radicals which are utilized in the CO oxidation. It is apparent from figure 3(*b*) that O_2 can leak through reaction (2) without being decomposed, leaving it in a form that is unusable for the main exothermic CO oxidation reaction, thus reducing the flame temperature. This becomes

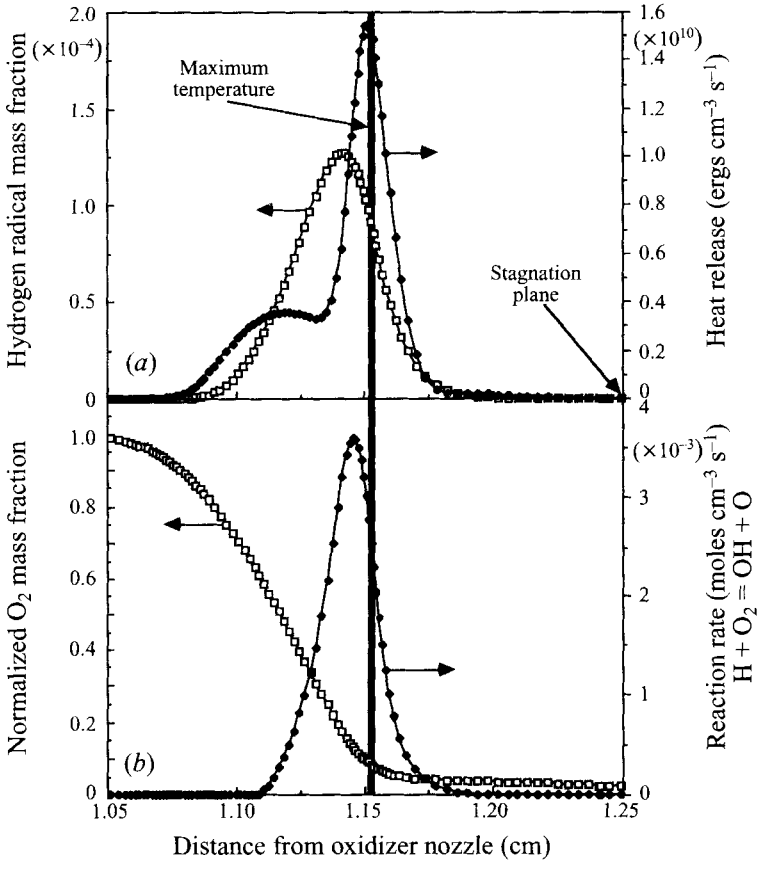

FIGURE 3. Structure of Flame I with $u_{exit} = 210$ cm s^{-1}. Spatial variations of (*a*) H mass fraction and heat release, and (*b*) O_2 mass fraction normalized by its free-stream value and reaction rate of main branching reaction $H + O_2 = OH + O$.

Flame		I	II	III	IV	V	VI
Nozzle separation distance (cm)		2.2	2.2	1.1	2.2	1.1	1.1
Nozzle mean exit velocity (cm s^{-1})		260	100	700	20	16	30
Nozzle exit velocity amplitude (cm s^{-1})		50	50	100	0	0	0
Nozzle mean exit temperature (K)		300	300	600	300	300	600
Nozzle exit temperature amplitude (K)		0	0	0	0	0	200
Oxidizer stream mean composition (% per mole)	O_2:	21.0	21.0	30.76	21.0	30.76	30.76
	N_2:	79.0	79.0	69.23	79.0	69.23	69.23
Amplitude of O_2 mole fraction (% in the oxidizer stream)		0	0	0	0	4.8	0
Fuel stream mean composition (% per mole)	CH_4:	71.4	71.4	71.4	71.4	71.4	71.4
	N_2:	28.6	28.6	28.6	28.6	28.6	28.6
Amplitude of CH_4 mole fraction (% in the fuel stream)		0	0	0	9.3	0	0
Mean strain rate on the oxidizer side (s^{-1})		400	149	2034	12	14	20

TABLE 1. Conditions of the diffusion flames studied herein

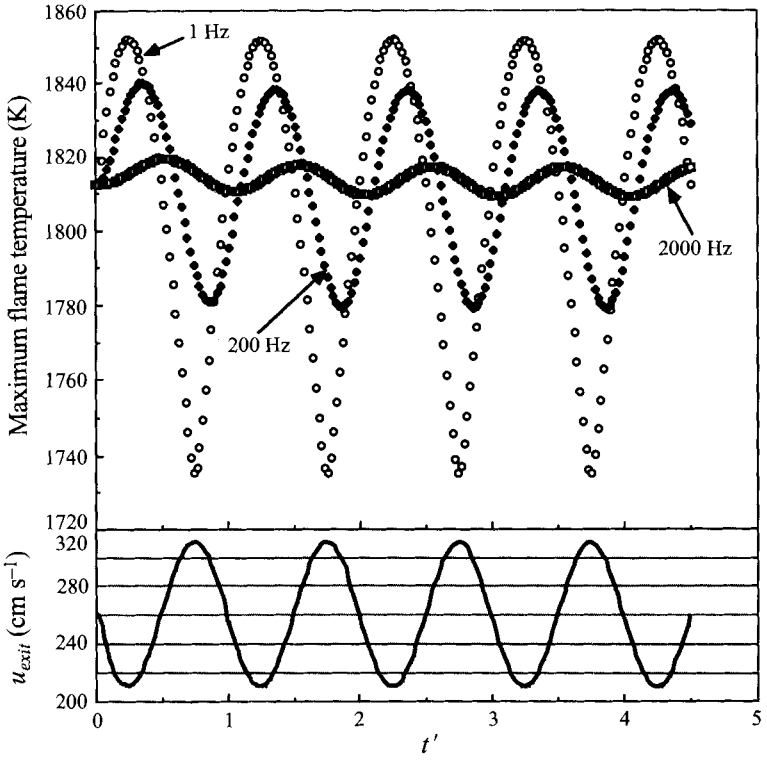

FIGURE 4. Variation of the maximum flame temperature, T_{max}, and nozzle exit reactant velocity, u_{exit}, with t' = time/period for Flame I at different frequencies.

more apparent as the strain rate increases and the transport of O_2 is augmented to a point that cannot be accommodated by the rate-limited kinetic step (2). The subsequent temperature reduction further weakens the high-activation-energy reaction (2) and causes additional O_2 leakage.

3.1. *Time-varying velocities at the nozzle exit*

For this portion of the investigation, velocity unsteadiness was introduced at the exit of both nozzles, while the free-stream values of reactant concentrations and temperatures were held fixed. Initially, the system is held in a steady state until $t = 0$ when the velocities begin to fluctuate following a sine function with damping. Furthermore, in all flames studied herein, the exit velocities from both nozzles have the same mean value and amplitude and oscillate in phase with one another. However, owing to the density differences of the two streams, the fluctuating momenta at the nozzles have different values and the location of the stagnation plane oscillates with time following the oscillation of the oxidizer stream which had, in all cases, higher momentum than the fuel stream; i.e. as the velocities increase, the stagnation plane moves further away from the nozzle from which the oxidizer is emerging.

The effect of unsteady nozzle exit velocity, u_{exit}, on the flame response was quantified for a wide range of conditions and among them three have been selected to be presented and discussed herein. For convenience, the classification Flames I, II and III will be used and the conditions for each flame are listed in table 1. In figures 4 and 5 results obtained for Flame I are reported. In figure 4 the variation of the maximum flame temperature, T_{max}, induced by the oscillation of u_{exit} is shown as a function of

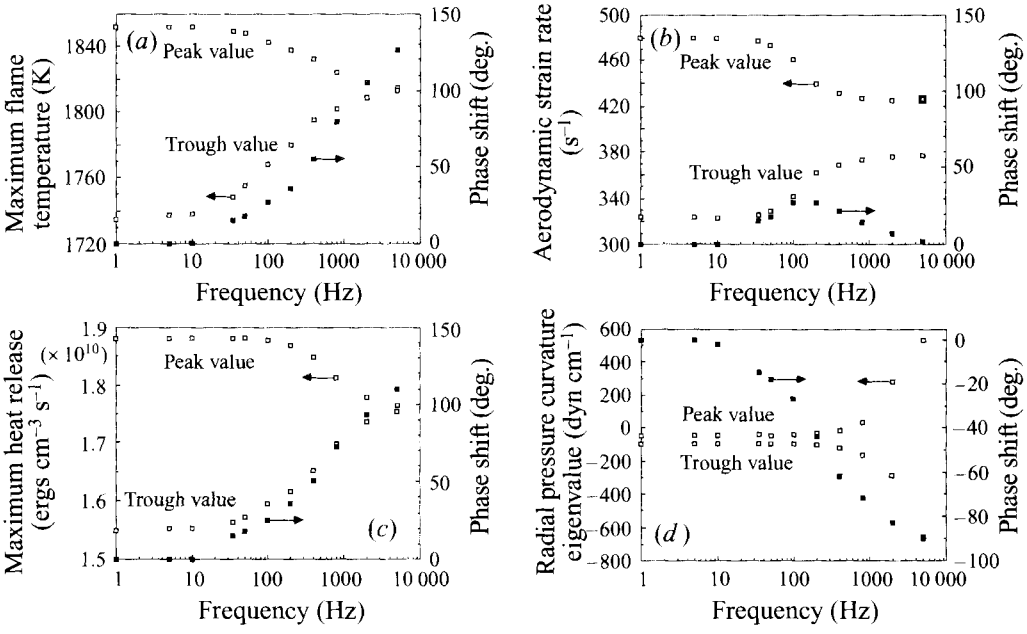

FIGURE 5. Detailed frequency response of the amplitudes of (*a*) the maximum flame temperature T_{max}, (*b*) the aerodynamic strain rate K, (*c*) the maximum heat release Q_{max}, and (*d*) the radial pressure curvature eigenvalue J, with their phase shifts for Flame I.

a non-dimensional time t', for different frequencies; the non-dimensional time t' results from the scaling of the dimensional time t by the period of oscillations. The results show that for higher frequencies the amplitude of oscillation decreases and the phase shifts to the right, in agreement with previous observations (Strahle 1965; Saitoh & Otsuka 1976; Stahl & Warnatz 1991; Cetegen & Bogue 1991; Cetegen & Pines 1992; Darabiha 1992; Ghoniem *et al.* 1992; Im & Law 1993; Im *et al.* 1995). Note that a constant burning rate despite the fact that the reactant delivery is unsteady implies that there must be some capacitive storage of reactants within the flame structure (see Appendix). Furthermore, T_{max} can be observed to vary asymmetrically about the mean value, especially at low frequencies.

The detailed frequency response of the peak and trough values of T_{max}, K, Q_{max}, and J are shown in figures 5(*a*)–5(*d*). The results mirror previous work in that the amplitude of oscillations is substantially reduced at higher frequencies while at low frequencies the flame responds to the u_{exit} time variations in a quasi-steady manner. It was also found that at low frequencies, the peak values of K, Q_{max} and J correspond to the peak values of u_{exit}, while the peak values of T_{max} correspond to the trough values of u_{exit}. Furthermore, the amplitude reduction occurs asymmetrically about the mean values for T_{max} and Q_{max}, with the trough values increasing faster than the reduction of the peak values. In contrast, the variations of the peak and trough values of K and J occur symmetrically about the mean values. At very high frequencies, the amplitude of T_{max} and Q_{max} approaches zero while K reaches a constant finite value; at the same time, the amplitude of J monotonically increases. Owing to the induced phase shift, u_{exit} leads T_{max}, K and Q_{max} but follows J. The phase shift of K disappears at low and high frequencies while the phase shift of J reaches $-90°$ at high frequencies. Note that the large amplitudes of J above 500 Hz are due to the large pressure gradients which are needed to obtain the large fluid accelerations at high frequencies.

Physically, the reduction of T_{max} at higher u_{exit} (and therefore higher K) is due to the increased O_2 leakage through the main reaction zone. Consequently, the extent of chain branching through reaction (2) is diminished resulting in a reduction of the overall exothermicity. Furthermore, higher values of u_{exit} result in higher burning rates and therefore higher Q_{max} and, as might be expected, higher K and J since they are directly related to the velocity gradients in space and time respectively.

The asymmetries about the mean observed in figures 4 and 5(*a*) occur because when u_{exit} (and consequently K) assumes its peak value, the O_2 leakage is enhanced. Therefore, the trough values of T_{max} are particularly sensitive to the reduction in the peak values of K at higher frequencies. This is also indicated in figure 4 as the trough values of T_{max} are more sharply pointed than the peak values. Similarly, the reduced straining results in a milder variation of T_{max} around its peak value compared to that around its trough value. The magnitude of Q_{max} is controlled by both the rate of reactant supply and the extent of exothermicity. The rate of reactant supply is mainly controlled by K while the exothermicity is controlled by reaction rates which are in turn determined by T_{max}. At higher frequencies, it was shown that while the peak and trough values of K merge symmetrically towards their mean value, the trough values of T_{max} increase at a faster rate than the reduction of its peak values. Therefore, the peak values of Q_{max} decrease at a noticeably slower rate than the increase of its trough values.

It should be noted at this point that the extent of the observed asymmetry depends on the amplitude of the imposed u_{exit} oscillations. More specifically, for the amplitudes of Flame I the trough and peak values of K cause noticeably different degrees of leakage of O_2 through the reaction (2) resulting in the observed asymmetry. For the same mean u_{exit} values, the calculations show that an increased amplitude of oscillations leads to a more profound asymmetry while a decreased amplitude leads to a more symmetric frequency response. This is reasonable since for reduced amplitudes the trough and peak values of K are closer and, therefore, lead to similar O_2 leakage.

We will now go on to explain the amplitude attenuation reported in figures 4 and 5 from first principles. But, before considering the effects induced by the flame, certain phenomena can be explained based on pure fluid mechanical arguments. First, as the frequency increases, the fluid experiences larger accelerations; consequently, the fluctuating magnitude of the driving pressure curvature J must also increase. This accounts for the observed phase shift as the motivation, J, must lead the response, u_{exit}. The response of the velocity field to u_{exit} variations is then straightforward. The flow field adjusts very rapidly to changes in u_{exit} since the imposed disturbances manifest themselves as pressure disturbances which propagate with the speed of sound and nearly instantaneously across the small (of the order of centimetres) distances studied here. Therefore, the changing mass flux information will be felt nearly instantaneously throughout the hydrodynamic zone.

Detailed analyses on the oxidizer side, well before the flame zone, show that the mass flux at any location in the hydrodynamic zone is in phase with u_{exit} at all frequencies. However, in the immediate vicinity of the flame, there will be a coupling between the fluid mechanics and the chemical/transport processes of the flame so that a phase shift is established between K and u_{exit} as the frequency increases. This shift results from the distortion of the local velocity field which results from thermal expansion which in turn, follows the phase-shifted T_{max}. At high frequencies, however, the phase shift of K approaches zero since the flame location and properties assume nearly constant values and thus exert a steady influence on K. Throughout this process, the only unsteady influence is u_{exit}, to which K responds nearly instantaneously. From figure

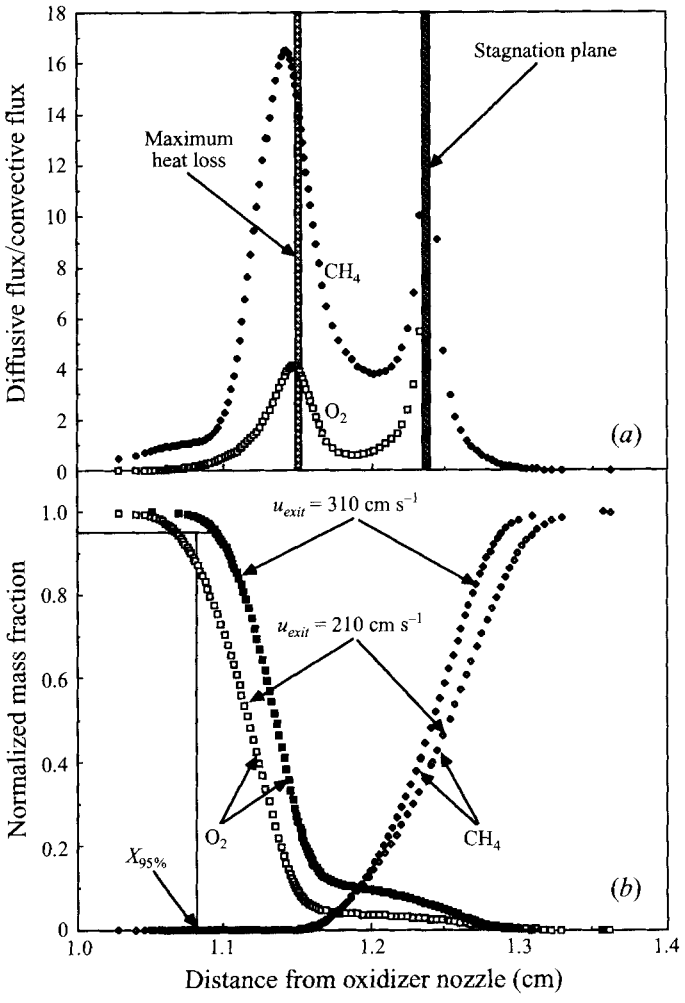

FIGURE 6. For Flame I and $f = 1$ Hz (*a*) variation of the ratio of diffusive over convective fluxes throughout the flame zone for the main reactants, and (*b*) variation of the reactant mass fractions throughout the flame zone normalized by their free-stream values and definition of the $X_{95\%}$ location.

5(*b*) it can be seen that the K-amplitude symmetrically approaches its asymptotic behaviour and it is only during this transition that the phase shift is apparent. The symmetry of the change in the amplitude of K is caused by its dominant dependence on u_{exit} which varies sinusoidally and thus oscillates symmetrically about its mean value.

In order to identify the elementary mechanisms responsible for the reduced flame response at high frequencies, it is necessary to understand the details of the flame structure. As stated above, the disturbances which are induced by u_{exit} oscillations will propagate nearly unchanged towards the flame through the hydrodynamic zone. Owing to the presence of the flame, the local structure includes regions in which diffusion is the dominant transport process for fuel, oxygen, and heat and a thin region between the two diffusion zones in which the main reaction activity takes place. Since the overall burning in a diffusion flame is largely controlled by the process of diffusion (as that is the main mechanism which brings the two reactants together), the diffusive zones are the 'bottlenecks' of the reactant transport. Thus the disturbances in the

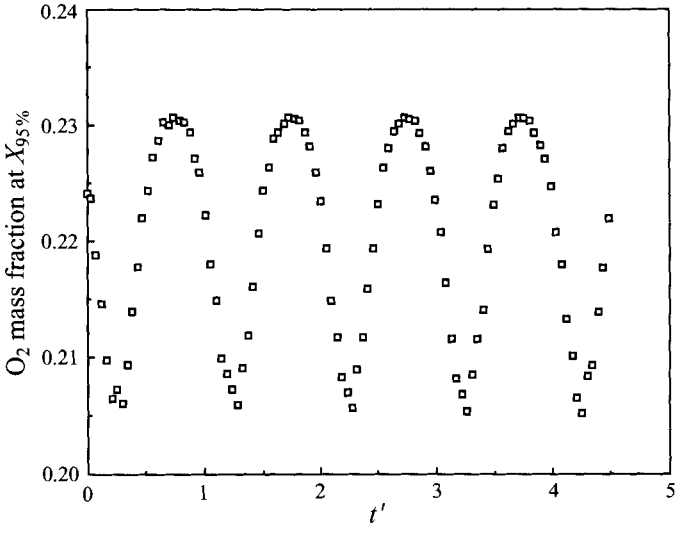

FIGURE 7. Variation of the O_2 mass fraction with t' = time/period at the spatial location $X_{95\%}$, for Flame I and $f = 1$ Hz.

hydrodynamic zone are only indirectly 'sensed' inside the reaction zone through the variations which the far-field disturbances induce on the mass diffusion processes; these diffusion processes occur in small but finite times which are much larger than the chemical reaction times. In figure 6(*a*), the spatial changes in the ratio of the diffusive to convective mass fluxes of the main reactants in the vicinity of the flame are shown. Diffusion is obviously dominant on both sides of the flame. This is a consequence of the very large spatial concentration gradients which develop in the flame's vicinity. (Note that local maxima in the ratio are also observed near the stagnation plane, but these are artifacts caused by the convective flux being nearly zero there which trivially leads to singular behaviour.)

Variations in u_{exit} result in variations of the mass flux exiting both nozzles and, therefore, variations in the burning rate. Since the final reactant transport into the flame occurs through diffusion, it is expected that if larger values of u_{exit} are to result in larger burning rates, they must induce larger reactant gradients in the diffusive zone. This can be seen in figure 6(*b*) for Flame I excited at $f = 1$ Hz, in which the mass fractions of O_2 and CH_4 (normalized by their free-stream values) are plotted versus the spatial location for the peak and trough values of u_{exit}. This indicates that the u_{exit} oscillations result in effective oscillations of the reactant mass fraction at the edge of the diffusive zone and this oscillation has to propagate largely by diffusion into the main reaction zone. A further graphic illustration of this point can be seen in figure 7 which shows the mass fraction of O_2 at a given location $X_{95\%}$. (The $X_{95\%}$ spatial location was determined as the mean location at which the mass fraction of O_2 is 95% of its free-stream value.) Therefore, the u_{exit} oscillations clearly result in oscillations of the reactant mass fractions at the outer edge of the reactant diffusive zones.

A close analogy is Stokes' second problem in which a plate oscillates within its plane under a stagnant fluid and the resulting fluctuating velocities 'penetrate' into the fluid through momentum diffusion. The amplitude of the velocity fluctuations scale spatially with a non-dimensional coordinate (White 1991)

$$\eta_z = z(\omega/2\nu)^{1/2},$$

where z is the dimensional distance from the plate, $\omega = 2\pi f$ the angular frequency, and ν is the kinematic viscosity of the fluid. In the Stokes problem, the amplitude of the induced velocity attenuates rapidly at large values of η_z (large z or large ω). That attenuation reflects the natural inclination of the diffusion process to even out spatial gradients of the parameter that motivates diffusion (i.e. velocity gradients in the Stokes problem and concentration gradients that feed the diffusion flames). At high frequencies, the short wavelength of the disturbances leads to large gradients and thus to large diffusive fluxes which are evened out by the diffusive process.

In the present problem there are reactant mass fraction oscillations at the outer edges of the diffusive zones, while the diffusive zones terminate in the main reaction region at which the mass fractions of both reactants are near-zero and change little with time. In analogy with the Stokes problem, the imposed mass fraction oscillation will be diffusively attenuated as it passes through the diffusive zone. At high frequencies, the amplitude of the oscillations can be substantially attenuated well before reaching the reaction zone, leading to reduced flame response.

There are, however, some differences between Stokes' second problem and the present one. First, the spatial extent over which the attenuation might be felt is limited to the size of the diffusive zones. Also, the oscillations occur not in a uniform system, but about large mean concentration gradients. (However, as Stokes' second problem is linear, its solution may be superposed over the concentration gradient to obtain an approximation to the conditions seen here.) And because both the flame and the outer edge of the diffusive zones move, the locations of the boundaries are not fixed. Finally, the temperature variations cause changes in the instantaneous mass diffusivities from values as low as 0.2 $cm^2\ s^{-1}$ to as much as 6 $cm^2\ s^{-1}$. However, while these effects may cause some quantitative changes in the scaling laws, they should not substantially affect the underlying physics. Therefore, as the frequency increases, the physical penetration length for oscillations will gradually become of the same order as the size of the diffusive zone so that the oscillations in the concentration gradients will be attenuated before they reach the flame. This, in turn, leads to the attenuated flame response.

The frequency response of Flames I, II, and III can be seen in figure 8 in which the normalized (by their quasi-steady values) amplitudes of T_{max} oscillations are shown as functions of frequency; Flames II and III correspond to lower and higher burning rates than Flame I, respectively. The results show that at low frequencies all flames behave in a quasi-steady manner with values of the normalized amplitude close to one; but at higher frequencies the amplitude decreases. However, the larger the burning rate, the higher is the frequency at which the amplitude becomes noticeably reduced. Physically, this occurs because, for higher burning rates, the reactant concentration gradients are larger and result in thinner diffusive zones, and thus a smaller distance on which the attenuation mechanism of Stokes' second problem can work.

To unambiguously demonstrate the Stokes' second problem analogy with the present one, the frequency response of Flames I, II, and III was further quantified in terms of the non-dimensional parameter $\eta_\delta = \delta(\omega/2D)^{1/2}$ instead of the frequency; for convenience, η_δ will be referred to as Stokes' parameter. (Note that, as heat must pass through the diffusive zone by conduction, the case of temperature fluctuations, which will be considered later in this paper, will be governed by a similar parameter in which the mass diffusion, D, is replaced by the thermal diffusivity, α). Here δ should be a measure of the thickness of the diffusive zones and we take it to be the mean spatial length between the 5% and 95% values of the reactant mass fractions. The diffusivity D is the average mass diffusivity within the same region. In figure 9(*a*) the variations of the normalized amplitudes of T_{max} oscillations are shown as functions of η_δ; here η_δ

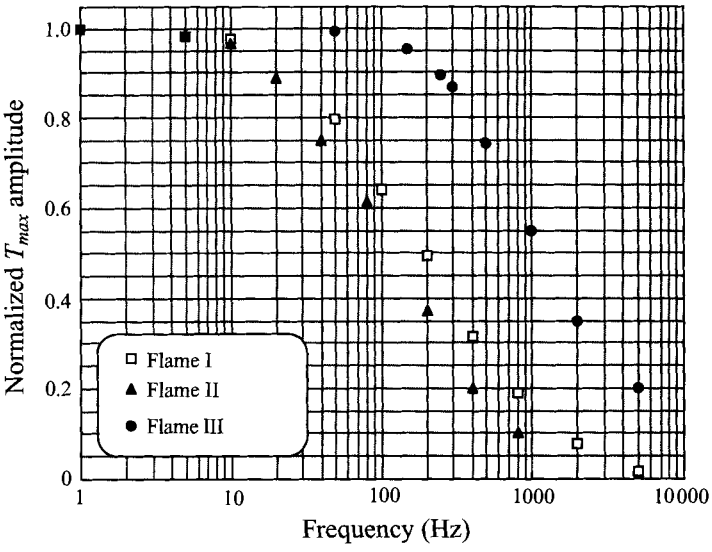

FIGURE 8. Variation of the T_{max} amplitude normalized by its quasi-steady value with frequency for Flames I, II, and III.

was determined separately for the fuel and oxygen diffusive zones properties. It is of interest to note that the results collapse close to a single curve, and that the choice of the fuel or oxygen for the scaling is not crucial (although the analogy is weaker on the oxidizer side as a small portion of the oxygen is transported through the flame by convection).

Unfortunately, quantities such as the thickness of the diffusion zone δ, while easily determined in the detailed studies presented here, are generally inaccessible, especially in experimental situations. However, it is possible to develop an equivalent parameter in terms of the strain rate, K (which may be estimated from the external stagnation flow). To begin the argument, note that at the outer edge of the diffusive zone the convective mass flux equals the diffusive mass flux:

$$\rho u Y_R = \rho D(\mathrm{d}Y_R/\mathrm{d}x),$$

where Y_R is the mass fraction of the main reactant. By further assuming that Y_R nearly vanishes at the boundary between the diffusive and reaction zones:

$$\rho D(\mathrm{d}Y_R/\mathrm{d}x) \approx \rho D(Y_R/\delta)$$

so that the balance at the interface between the diffusion and reaction zones becomes

$$\rho u Y_R \approx \rho D(Y_R/\delta).$$

In a uniform straining flow the velocity at the edge of the diffusive zone can be estimated from inviscid theory:

$$u = K\delta,$$

and combining with the mass flux balance equation leads to

$$\delta \approx (D/K)^{1/2}.$$

Thus a parameter equivalent to η_δ may be defined as

$$\eta_K = (\omega/2K)^{1/2}.$$

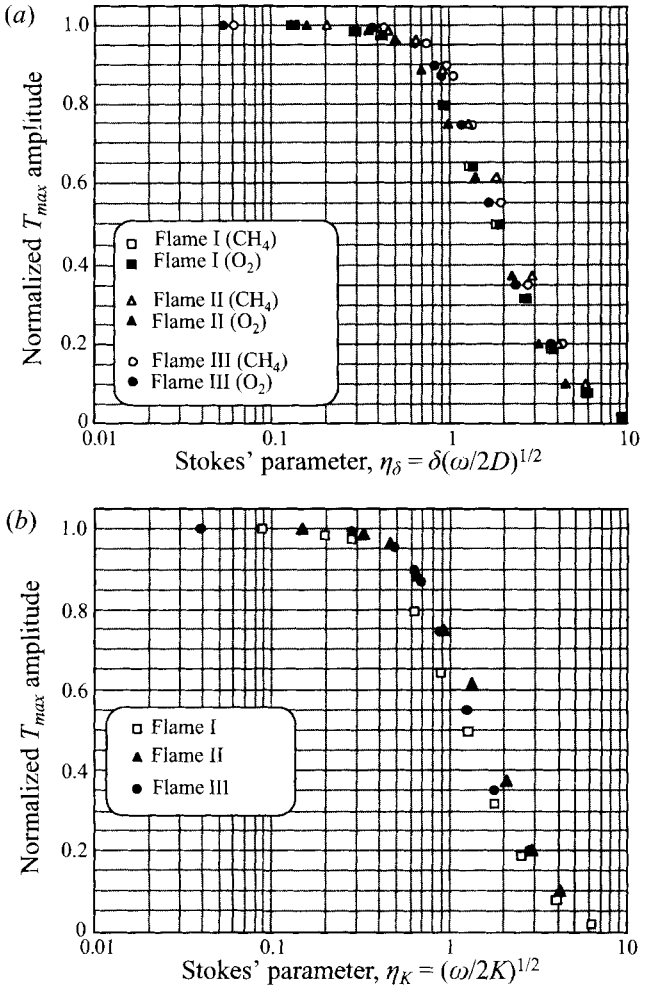

FIGURE 9. Variation of the T_{max} amplitude normalized by its quasi-steady value for Flames I, II, and III with (*a*) the parameter η_δ defined in terms of the angular frequency, ω, and the properties of the diffusive zones, and (*b*) the parameter η_K defined in terms of the angular frequency, ω, and the aerodynamic strain rate, K.

In figure 9(*b*) the variation of the normalized amplitudes of T_{max} oscillations are shown as functions of η_K and again it can be seen that the results collapse to a single curve that is nearly identical to that obtained by plotting against η_δ shown in figure 9(*a*). This is a clear indication that η_δ and η_K are numerically equivalent parameters. The data of figure 9 indicate that η is an appropriate non-dimensional parameter that controls the frequency response of the flame. It is also of interest to note that the drastic drop of the normalized temperature amplitude starts for values of η around one. This is physically sound since when $\eta = O(1)$, the characteristic diffusion length δ is of the same order as the characteristic penetration length so that the 'attenuation' effect should significantly influence the structure in the diffusive zone. Therefore, the characteristic angular frequency at which substantial attenuation commences is of the order of

$$\omega \approx 2D/\delta^2 \approx 2K,$$

where δ and K correspond to the average value of u_{exit} throughout the cycle.

Note that while the above arguments are written in terms of mass diffusion, they could be repeated nearly identically for heat transfer problems by replacing the species mass fraction Y_R by the temperature rise, $T_{max}-T_u$, from the unburned mixture temperature, T_u, to T_{max}, and the mass diffusivity D by the thermal diffusivity α. That calculation would result in exactly the same parameter, η_K. In other words the value of the Lewis number (α/D) does not affect the derivation of η_K. Thus, η_K may be considered to be a universal parameter describing the frequency response of the flame to the fluctuation of all three quantities, velocity, concentration and temperature, that are studied in this paper.

The imposed reactant concentration oscillations at the beginning of the diffusive zones also explain the observed phase shift of the flame properties at high frequencies. Since a small but finite time is needed for the reactant molecules to be transported to the main reaction zone through diffusion, it is reasonable to expect that the main reaction zone will respond at a later time to concentration perturbations at the outer edge of the diffusion zone. In examining the totality of the data it was apparent to the authors that this 'diffusive' time corresponds to the observed phase shift; this is more noticeable at higher frequencies for which this time becomes a large fraction of the period.

3.2. *Time-varying reactant concentration at the nozzle exit*

To demonstrate that the diffusion-limited concept has wide validity, further studies were performed for which the fluid velocity and temperature are held fixed while the reactant concentrations at the nozzles are varied with time. In some cases, the CH_4 mole fraction is oscillated and in others, the O_2 mole fraction, but never the two together. The mean conditions about which the concentrations are varied are shown in table 1.

For the conditions of Flame IV the CH_4 mole fraction at the exit of the fuel stream nozzle $X_{CH_4,exit}$, was varied periodically around a mean value following a cosine function so that the steady solution corresponds to the top of the cycle; at the same time, the O_2 mole fraction at the exit of the oxidizer nozzle was kept constant. It was found that the peak value of T_{max} occurs when $X_{CH_4,exit}$ is at its peak value which is physically sound since T_{max} increases with the free-stream reactant concentrations. The dependence of T_{max} on the frequency of oscillations is shown in figure 10 and, as for the flame's response to u_{exit} oscillations, it can be seen that the T_{max} amplitude is reduced and a substantial phase shift is established as the frequency increases. Again, analysis of the detailed flame structure showed that the phase shift is caused by the finite value of the total transport time (through convection and diffusion) that it takes CH_4 molecules to pass from the nozzle exit to the main reaction zone.

For the conditions of Flame V, the O_2 mole fraction at the exit of the oxidizer stream nozzle $X_{O_2,exit}$, was varied periodically around a mean value while the CH_4 mole fraction at the exit of the fuel nozzle was kept constant. Similarly to the $X_{CH_4,exit}$ oscillations, it was found that the peak value of T_{max} occurs when the $X_{O_2,exit}$ is at its peak value. The dependence of T_{max} on the frequency of oscillations is similar to that of figure 10 for Flame IV, namely that T_{max} amplitude is reduced and a substantial phase shift is established as the frequency increases.

In order to explain the frequency response of Flames IV and V to free-stream reactant concentration oscillations, a similar approach to that of §3.1 was taken. As expected, it was found that for both cases the reactant concentration oscillation at the nozzle exit leads to reactant concentration oscillation at the beginning of the main transport zone so that the analogy with Stokes' second problem is still valid. To demonstrate this, the amplitudes of T_{max} oscillations (normalized by their quasi-steady

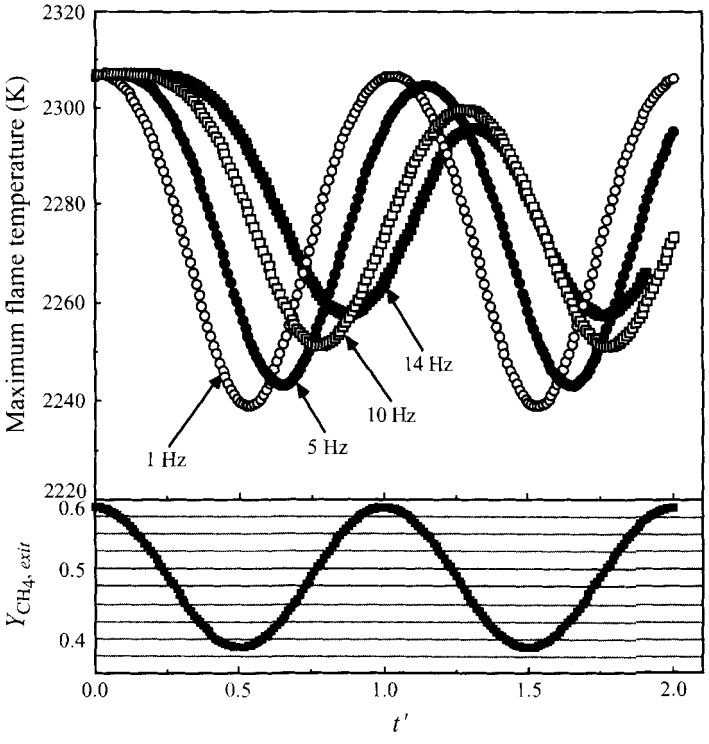

FIGURE 10. Variation of the maximum flame temperature, T_{max}, and methane mass fraction at the fuel nozzle exit, $Y_{CH_4,exit}$, with t' = time/period for Flame IV at different frequencies.

values) are shown in figure 11 as functions of Stokes' parameter, η_K. It is obvious that the results obtained by oscillating CH_4 are very close to those obtained by oscillating O_2 and that the amplitude reduction is substantial when $\eta_K = O(1)$, once again in agreement with the results of figure 9.

Unlike, the fluctuating velocity case, fluctuating the concentration sets up concentration gradients throughout the convective zone as well as the diffusive zone. Thus it is possible that diffusive attenuation may occur long before the flame is approached. However, this part of the attenuation is not associated with the flame structure, but instead depends on the size of the convective zone between the nozzle exit and the start of the diffusive zone. This depends not on the local structure of the flame but on external characteristics such as the size L of the apparatus and is thus not important in understanding the flame behaviour. Such attenuation was apparent in that the fluctuation amplitude at the beginning of the diffusion zone was clearly smaller than at the nozzle exits; unfortunately it is difficult to quantifiably connect those observations to the flame response. The attenuation in the convective zone will be a function of frequency ω, as ω (along with the exit velocity) governs the spatial gradients in the convective zone that drive diffusive attenuation. Also, it will depend on the strain rate K, which affects the relative size of the convective and diffusive zones (e.g. small K means a large diffusive and a small convective zone). Thus at small K it is possible to eliminate the effects of attenuation in the convective zone due to its reduced size, and we have thus used small strain rates from Flames IV, V (and VI). (At higher strain rates, the behaviour is qualitatively the same except that the reduction occurs at smaller values of η_K.)

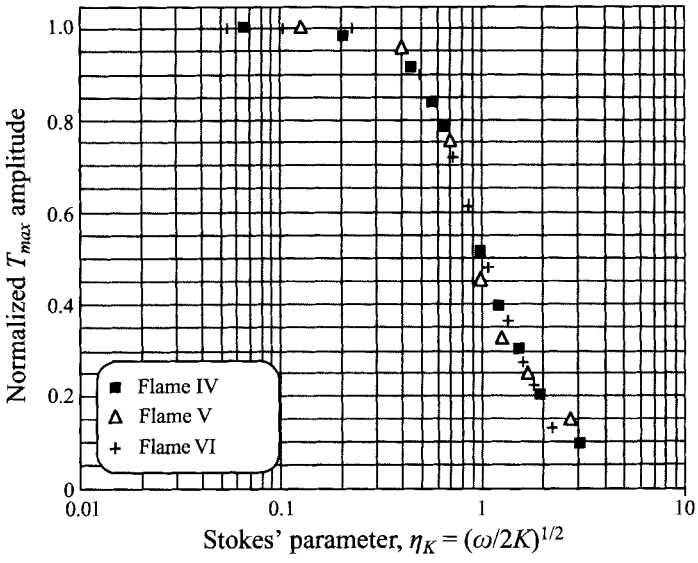

FIGURE 11. Variation of the T_{max} amplitude normalized by its quasi-steady value for Flames IV, V, and VI with the parameter η_K defined in terms of the angular frequency, ω, and the aerodynamic strain rate, K.

3.3. *Time-varying reactant temperature at the nozzle exit*

In a turbulent flow, a flamelet will be exposed to time-varying temperatures in addition to the time varying velocities and concentrations. Now, the temperature variations will have several effects on a flamelet. First of all, a temperature increase will increase the reaction rates so that any available reactants will be consumed more quickly. However, it will also decrease the local density, both in the bulk and for the individual reactants surrounding the flamelet; in a sense, this reduces the mass of the reactants available to the flame. Finally, it will also change the material properties; the viscosity, conductivity and specific heats will all rise with temperature and may affect the thermal response of the gas.

To try and isolate the effect of temperature fluctuations, the initial unburned temperature values leaving the nozzle exits T_{exit}, were oscillated while keeping the reactant nozzle exit velocities and concentrations constant. (Here as in §3.2, initial transients were eliminated by having the imposed oscillations initially follow a cosine connecting to a sine function.) Furthermore, for all flames studied herein the exit reactant temperatures from both nozzles have the same mean value and both are oscillated with the same amplitude and in phase with one another. The conditions of this study are shown in table 1 under Flame VI and the temporal response of the maximum temperature can be seen in figure 12.

As might be expected, it was found that the peak value of T_{max} occurs when the T_{exit} is at its peak value. But notice that, even for the quasi-steady cases, the amplitude of the maximum temperature variation is smaller than the 200 K amplitude at the nozzle exits. One would expect that if there were no response from the flame, the magnitude of flame temperature oscillations will be at least as large as the fluctuation in the environment temperature induced at the nozzle. This is key to understanding the driving forces behind the flame response. If the dominant effect were the variations in reaction rates with temperature, then one would expect that the exothermicity would increase when the feed temperature was high and decrease when the feed temperature

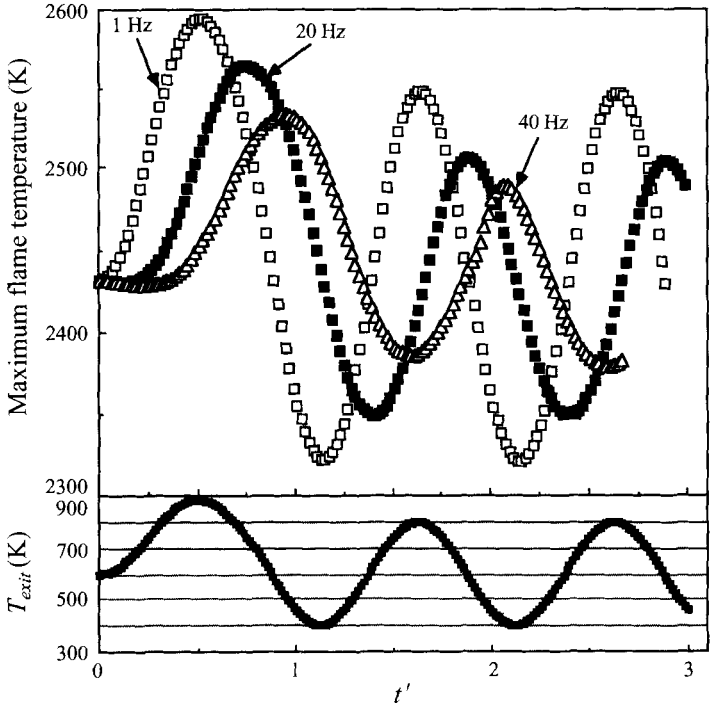

FIGURE 12. Variation of the maximum flame temperature, T_{max}, and nozzle exit reactant temperature, T_{exit}, with t' = time/period for Flame VI at different frequencies.

was low so as to generate larger temperature fluctuations. The fact that the flame amplitude is smaller when the temperature is large, indicates that the reaction rate effect is not dominant here. In fact, if one were to plot the heat release as a function of time, one would see that the exothermicity is indeed out of phase with the driving temperature by precisely this mechanism. However, that should not be reflected in the temperature as it is easy to show that the extra heat released must go to raise the temperature of the extra mass; as the extra heat generated and the extra heat capacity are both proportional to the extra mass, no additional rise in temperature will occur. Instead, the temperature response seen here is a result of the change in the specific heat of the mixture. At large feed temperatures, the specific heat of the material is larger (this is particularly true for the methane side) so that the reaction exothermicity produces a smaller temperature response. But notice that the amplitude of the response is also reduced as the frequency increases, much as for the velocity and concentration effects discussed above, indicating that a similar effect may also be present. Furthermore a substantial phase shift can be observed with increased frequency. Analysis of the detailed flame structure showed that the phase shift is once again caused by the magnitude of the total transport time (through convection and diffusion) of the thermal energy from the exit of the nozzle to the flame zone.

It should not be surprising that this effect is similar to those for velocity and concentration. After all, heat obeys a diffusion equation similar to that for mass diffusion. But there still are differences between the two problems. In particular, the flame acts as a source of heat while it is a sink of mass. But other than that the thermal structure is similar to the mass diffusion structure. As can be seen in figure 2, there are large temperate gradients in the immediate vicinity of the flame within which molecular

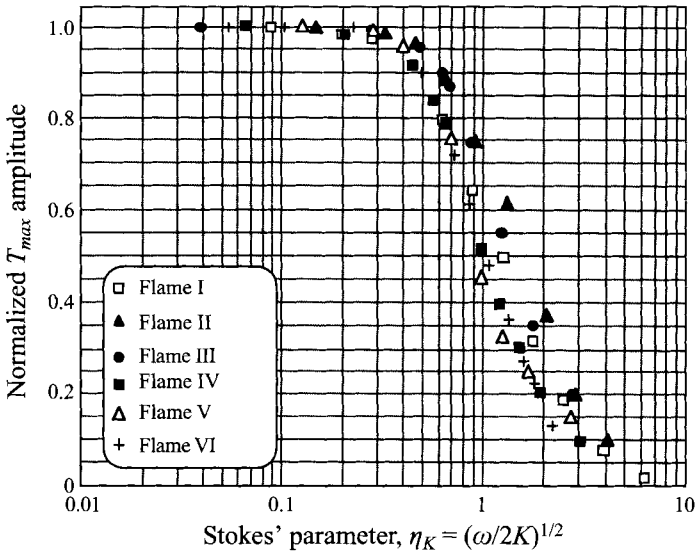

FIGURE 13. Variation of the T_{max} amplitude normalized by its quasi-steady value with the parameter η_K for Flames I–VI.

conduction will be the dominant transport mechanism; farther away from the flame the gradients are small and convection will dominate. The same diffusion-induced attenuation will take place within the conduction zone. Making an analogy with the above discussion, one would expect that the attenuation would depend on a parameter $\eta_{\delta_T} = \delta_T(\omega/2\alpha)^{1/2}$, where δ_T is the thermal boundary layer thickness and α is the thermal diffusivity. However, if one goes through the same type of analysis as in §3.1, one finds that $\delta_T \approx (\alpha/K)^{1/2}$. Making that substitution, one finds that $\eta_{\delta_T} \approx \eta_K$ and since we have already shown that $\eta_\delta \approx \eta_K$ it implies that $\eta_{\delta_T} \approx \eta_\delta$: i.e. that η_{δ_T} and η_δ should have approximately the same numerical values. This is clearly illustrated in figure 11 which shows the data for Flames IV and V (concentration oscillations) as well as for Flame VI (thermal oscillations). Clearly, the curves are nearly indistinguishable.

The arguments demonstrate that η_K is a universal parameter that describes the diffusion-limited frequency response (be it thermal or mass diffusion) of diffusion flames. To illustrate this point, in figure 13 the dependence of the normalized flame temperature amplitude data on η_K for all cases studied herein is shown. Clearly the attenuation behaviour for all cases, be it fluctuating velocity, concentration or temperature scales closely with η_K.

4. Concluding remarks

In the present investigation, two major objectives were accomplished. The first was to perform a detailed numerical simulation of unsteady strained methane/oxygen/nitrogen diffusion flames in a finite-domain counterflow. The simulation was conducted for a wide range of unsteady conditions for the reactant velocity, concentrations, and temperature imposed at the nozzle exits, with the hope that the data will lead to understanding turbulent combustion in the laminar flamelet regime. Furthermore, as they were performed in a realistic finite domain, these results can effectively guide future experimental studies. The second objective was to provide

enhanced insight from first principles into the elementary mechanisms that control the flame's frequency response.

The results of the numerical simulation show that the flame's response depends on the frequency of the applied oscillations. At low frequencies, the flame properties follow the externally imposed oscillations in a quasi-steady manner. But at high frequencies, a phase shift is established between the forced oscillations and the flame response and, at the same time, the induced oscillations of the flame properties are reduced. As the frequency is further increased, all properties asymptotically merge towards mean values.

The analysis of the instantaneous flame structure revealed the mechanisms responsible for the reduced flame response at high frequencies. It was found that the imposed oscillations in the hydrodynamic zone result in reactant concentration and temperature oscillations inside the diffusive zone adjacent to the flame. Such phenomena are analogous to Stokes' second problem and the response to velocity fluctuations was found to scale with the non-dimensional parameter $\eta_\delta = \delta(\omega/2D)^{1/2}$. The same parameter should also determine the response to concentration fluctuations and an equivalent parameter (formed by replacing the mass diffusivity D, by the thermal diffusivity α, and the diffusional thickness δ by the corresponding thermal thickness δ_T) governs the response to temperature fluctuations. However, it was shown that both parameters should be numerically almost equal to a universal parameter $\eta_K = (\omega/2K)^{1/2}$, which relates the local fluid mechanics to the flame's response to fluctuations in velocity, concentration or temperature. The results show that, for all cases studied herein, the amplitude of the flame response scales very closely with η_K, and that when $\eta_K = O(1)$ substantial amplitude attenuation is observed.

In a true turbulent environment, a flamelet will be simultaneously subjected to time-varying strain rate, concentration and temperature. In this paper, each effect has been considered separately although it is possible that there is coupling between the various fluctuating quantities. However, unless such couplings are dominant, the current results indicate that the frequency response of flamelets is governed by a single parameter η_K, and that, for the large η_K, flamelets will be insensitive to turbulent fluctuations. The parameter η_K depends only on the imposed angular frequency ω, and the strain rate K, both of which are properties of the local turbulence which, on the scales of flamelets, may be dominated by a small number of small-scale eddies. Consequently, it may be possible that there are turbulent events for which the combustion is relatively insensitive to temporal variations of any properties.

F.N.E. was supported by the National Science Foundation under Grant CTS-9211844 while C.S.C. was supported by the US Department of Energy under grant DE-FG03-91ER14223.

Appendix. Flame structure under time-varying reactant velocities

In the course of these investigations, we made an interesting observation of the effects of velocity fluctuations on the flame structure. This will be illustrated using Flame I which is described in table 1. As it was observed that this flame responds quasi-steadily to low-frequency oscillations and is unresponsive to high-frequency oscillations, the corresponding changes in the flame structure will be observed by comparing the results of forcing the flame at frequencies of 1 and 2000 Hz.

The effect of the frequency of the velocity fluctuations on the flame structure is

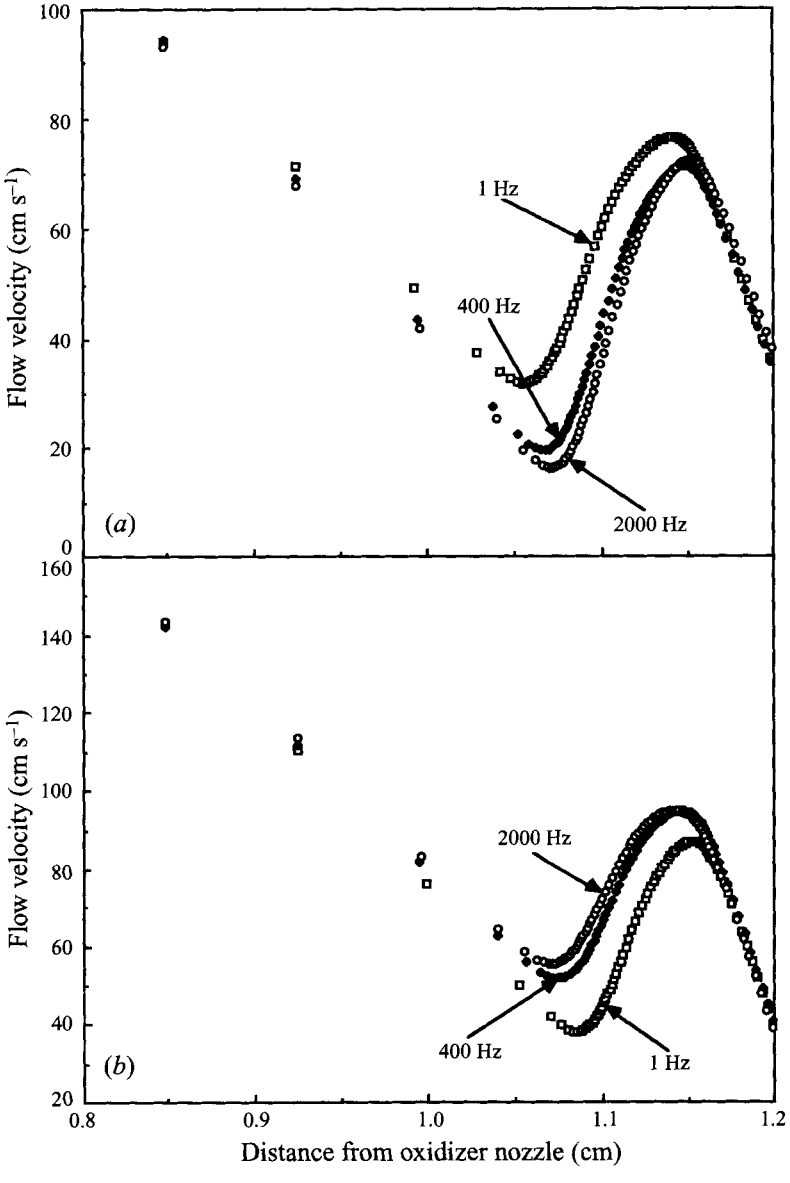

FIGURE 14. Variation of the flow velocity throughout the flame zone for Flame I at various frequencies for (*a*) $u_{exit} = 210$ cm s^{-1} and (*b*) $u_{exit} = 310$ cm s^{-1}.

shown in figures 14–16. Basically, these counterflow diffusion flames can be divided into three spatial regions: (i) a convective region far from the flame in which the flow is largely incompressible and convection is largely responsible for the reactant delivery, (ii) a diffusion zone very near the flame, in which the concentration gradients large so that diffusion is largely responsible for reactant transport, and (iii) an interface between these two regions. In figure 14, the effect of frequency on the fluid mechanics near this interface zone is shown. Figure 14(*a*) depicts the velocity profile when u_{exit} is at its trough value while figure 14(*b*) depicts the profiles when u_{exit} is at its peak value for Flame I. It is clear that the local velocity gradient before the main diffusive zone (which is represented by the aerodynamic strain rate K) is strongly affected by the frequency

of the imposed oscillations. (Note that here, the end of the approximately isothermal portion of the convective zone is marked by the local velocity minimum; beyond this point the velocity increases due to the density reduction induced by heating from the flame. Thus K is determined in the region immediately before this minimum.) It is clear from this figure that K oscillates at low frequencies with a larger amplitude than at high frequencies. When u_{exit} is at its trough value, the corresponding value of K increases with frequency; the opposite is true when u_{exit} is at its peak value where K can be seen to decrease with increasing frequency. It was shown above that the flame is unresponsive to high-frequency oscillations in general and thus to oscillations in K in particular. But if the flame is unresponsive at high frequencies (i.e. it exhibits a constant burning rate) then it must be fed a constant supply of reactants, regardless of the reactant supply in the far field.

Along those lines, figure 15(*a*) and 15(*b*) depict the total (convective+diffusive) fluxes of O_2 and CH_4 for the conditions corresponding to the peak (310 cm s^{-1}) and trough (210 cm s^{-1}) values of u_{exit} for the case of Flame I at $f = 1$ Hz and $f = 2000$ Hz respectively. At $f = 1$ Hz (figure 15*a*) there are very noticeable differences between the trough and peak flux profiles, indicating that the oscillations propagate through the diffusive zones and are sensed by the reaction zone. On the other hand, at $f = 2000$ Hz (figure 15*b*) the flux profiles are clearly different far from the flame in the region where convection dominates, but inside the diffusive zone the profiles merge, indicating nearly uniform mass delivery and, consequently, uniform burning rate. This observation raises an obvious point: as more mass (of fuel or oxidizer) is delivered than is consumed by the flame at the peak if the oscillation, while less mass is delivered than is consumed during the troughs, the structure must accumulate mass during the peaks and deliver it during the troughs, i.e. there are mechanisms inherent to this structure that behave much like a capacitor in an electrical circuit. Note that in figure 15(*b*), positive mass flux gradients of O_2 may be seen near the edge of the diffusion zones (in the region between about 1.07 and 1.12 cm from the oxidizer nozzle) when the velocity is at its trough value (210 cm s^{-1}). This indicates that more oxygen is being delivered to the flame than is being delivered in the convection zone far from the flame. This is a clear demonstration of a capacitive effect in the diffusion zone. As the diffusion zone ultimately controls the rate of reactant feed to the flame, its effect may be thought of as resistive. The capacitance at the interface combines with the resistive effects of the diffusion zone to create a fluidic resistance-capacitance low-pass filter that could partially attenuate the high-frequency oscillations.

It can be seen from the mass conservation equation that the mass accumulation can only be induced by a non-zero time variation of the density. Under the conditions of near-constant pressure seen here (the pressure is largely determined by the far-field atmospheric pressure) density variations can only be induced by temperature variations. (As the mixtures are largely diluted by nitrogen, concentration changes can only have a negligible effect on the overall density.) Thus, the density does not change within the main hydrodynamic zone within which only the flow velocities vary. Furthermore, at high frequencies there are no property variations within the main diffusive zone since the flame does not respond to the imposed oscillations, and is stabilized at a nearly fixed location with nearly fixed properties throughout the duration of the cycle. Consequently, the observed capacitive effect implies that the temperature must vary with time along the interface between the hydrodynamic and the diffusive zones. The amplitude of the temperature oscillations is shown as solid points in figure 16. These temperature variations lead to temporal variations of the local density (which become more noticeable at higher frequencies).

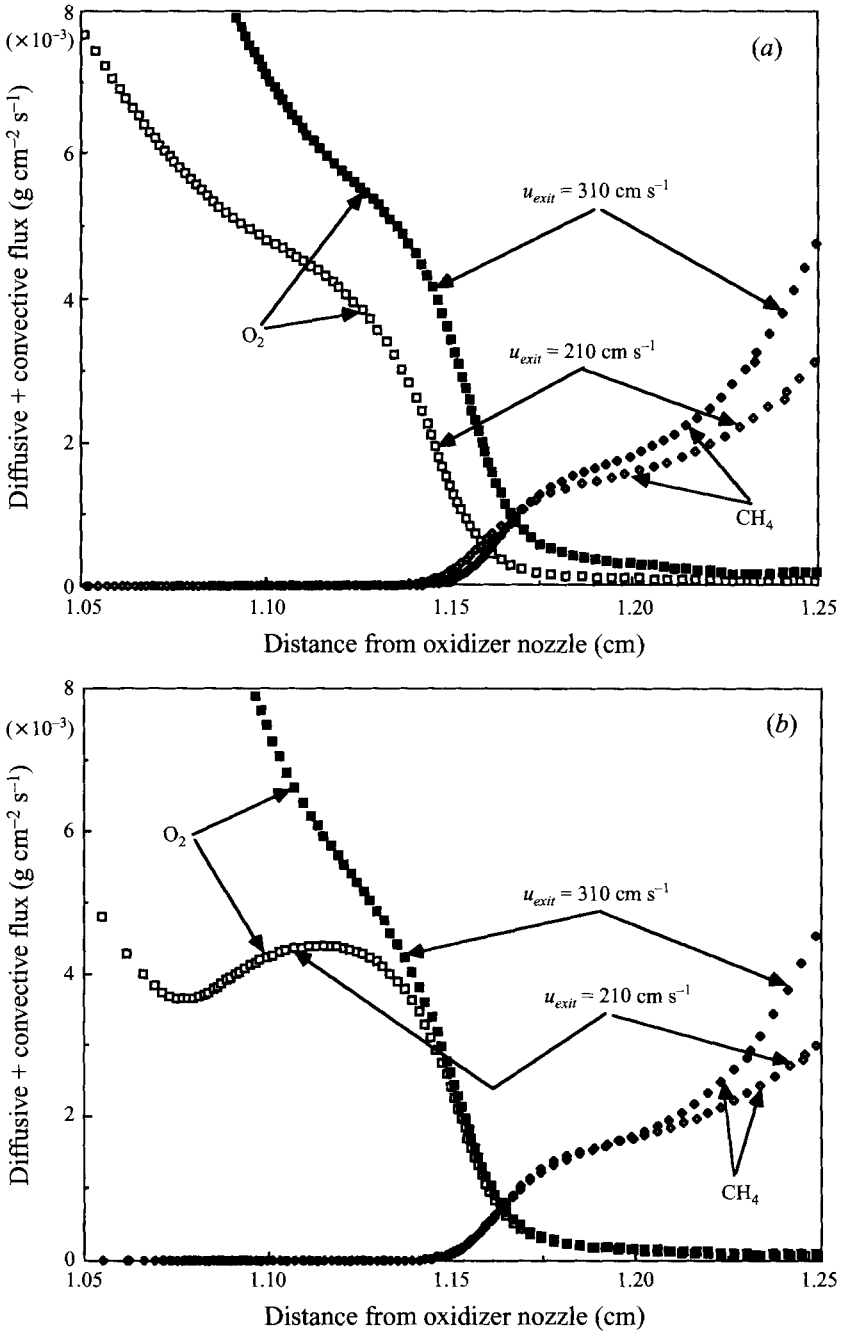

FIGURE 15. Variation of the total (diffusive+convective) reactant fluxes throughout the flame zone, for Flame I and for $u_{exit} = 210$ cm s^{-1} and $u_{exit} = 310$ cm s^{-1} at (*a*) $f = 1$ Hz, (*b*) $f = 2000$ Hz.

Physically, the mechanism that results in the mass accumulation is induced by the inability of the flame to move at high frequencies. But even though the flame is located at a fixed position it encounters variable mass fluxes issuing from the nozzles. Since at high frequencies the flame temperature and all lengthscales of the system are fixed, the amount of heat transfer from the flame is constant. Since u_{exit} oscillates, an oscillating

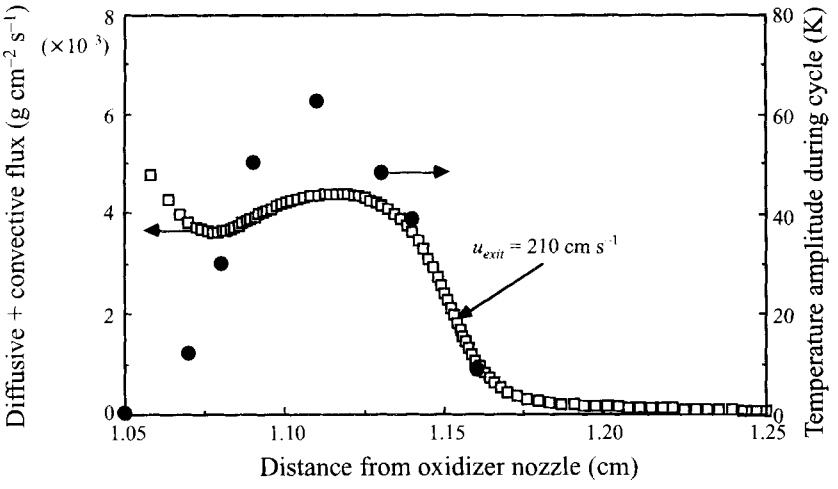

FIGURE 16. Variation of the total (diffusive + convective) reactant flux of O_2 at the interface between the hydrodynamic and diffusive zones for Flame I and for $u_{exit} = 210$ cm s^{-1} at $f = 2000$ Hz and the amplitude of the oscillations of the local temperature.

mass flux passes the interface between the hydrodynamic and diffusive zones. The oscillating mass flux implies that the constant heat flux to which it is exposed will cause larger temperature rises when the mass flux is small than when the mass flux is large; this will result in oscillating temperatures even though the burning rate is constant. In turn, the oscillating temperatures result in oscillating densities and consequently in the capacitive mass accumulation. Thus when the incoming mass flux is large the interface temperature is small and the density is large; thus mass is accumulated at the interface during the peaks of the velocity fluctuations. When the mass flux is small, the interface temperature is large and the density is small; hence mass is expelled from the interface region during troughs in the velocity fluctuations.

The above discussion suggests an alternative mechanism to explain the frequency attenuation in cases where the reactant velocities are oscillated. This begs the question as to whether this accumulation mechanism or diffusion limitation is actually responsible for the observed attenuation. But the answer is obvious as the scaling with η_δ shows that the attenuation scales with diffusion quantities. As it is unlikely that the mass accumulation mechanism shown in this Appendix will scale with the diffusivity, the resulting attenuation must be relatively unimportant relative to that imposed by diffusion. One should also note that no similar mechanism was observed when the reactant concentration or temperature was the oscillated quantity. Thus diffusional attenuation appears to be the dominant mechanism governing the frequency response of these flames.

REFERENCES

BRACCO, F. V. 1988 Structure of flames in premixed-charge IC engines. *Combust. Sci. Tech.* **58**, 209.

CARRIER, G. F., FENDELL, F. E. & MARBLE, F. E. 1975 The effect of strain rate on diffusion flames. *SIAM J. Appl. Maths* **28**, 463–499.

CETEGEN, B. M. & BOGUE, D. R. 1991 Combustion in a stretched fuel strip with finite rate chemistry. *Combust. Flame* **86**, 359–370.

CETEGEN, B. M. & PINES, D. S. 1992 Combustion of a stretched carbon monoxide ligament with radiative heat losses. *Combust. Flame* **91**, 143–152.

CHELLIAH, H. K., LAW, C. K., UEDA, T., SMOOKE, M. D. & WILLIAMS, F. A. 1990 An experimental

and theoretical investigation of the dilution, pressure and flow-field effects on the extinction condition of methane–air–nitrogen diffusion flames. *Twenty-Third Symp. (Intl) on Combustion*, pp. 503–511. The Combustion Institute.

CLARKE, J. F. & STEGEN, G. R. 1968 Some unsteady motions of a diffusion flame sheet. *J. Fluid Mech.* **34**, 343–358.

DARABIHA, N. 1992 Transient behaviour of laminar counterflow hydrogen–air diffusion with complex chemistry. *Combust. Sci. Tech.* **86**, 163–181.

DIXON-LEWIS, G. 1990 Structure of laminar flames. *Twenty-Third Symp. (Intl) on Combustion*, pp. 305–324. The Combustion Institute.

EGOLFOPOULOS, F. N., CHO, P. & LAW, C. K. 1989 Laminar flame speeds of methane–air mixtures under reduced and elevated pressures. *Combust. Flame* **76**, 375–391.

EGOLFOPOULOS, F. N., DU, D. X. & LAW, C. K. 1992 A comprehensive study of methanol kinetics in freely-propagating and burner-stabilized flames, flow and static reactors, and shock tubes. *Combust. Sci. Tech.* **83**, 33–75.

EGOLFOPOULOS, F. N. & LAW, C. K. 1990 Chain mechanisms in the overall reaction orders in laminar flame propagation. *Combust. Flame* **80**, 7–16.

EGOLFOPOULOS, F. N. & LAW, C. K. 1994 Further considerations on the methanol oxidation kinetics. In preparation.

GHONIEM, A. F., SOTERIOU, M. C., CETEGEN, B. M. & KNIO, O. M. 1992 Effect of steady and periodic strain on unsteady flamelet combustion. *Twenty-Fourth Symp. (Intl) on Combustion*, pp. 223–230. The Combustion Institute.

HAWORTH, D. C., DRAKE, M. C., POPE, S. B. & BLINT, R. J. 1988 The importance of time-dependent flame structures in stretched laminar flamelet models for turbulent jet diffusion flames. *Twenty-Second Symp. (Intl) on Combustion*, pp. 589–597. The Combustion Institute.

IM, H. G. & LAW, C. K. 1993 Response of counterflow diffusion flame to oscillating strain rates. *Technical Meeting of the Eastern States Section of The Combustion Institute*, Paper 99, Princeton University, Princeton, NJ.

IM, H. G., LAW, C. K., KIM, J. S. & WILLIAMS, F. A. 1995 Response of counterflow diffusion flame to oscillating strain rates. *Combust. Flame* **100**, 21–30.

KEE, R. J., MILLER, J. A., EVANS, G. H. & DIXON-LEWIS, G. 1988 A computational model of the structure and extinction of stretched, opposed flow, premixed methane–air flames. *Twenty-Second Symp. (Intl) on Combustion*, pp. 1479–1494. The Combustion Institute.

KEE, R. J., RUPLEY, F. M. & MILLER J. A. 1989 Chemkin-II: A Fortran chemical kinetics package for the analysis of gas-phase chemical kinetics. *Sandia Rep.* SAND89-8009.

KEE, R. J., WARNATZ, J. & MILLER J. A. 1983 A FORTRAN computer code package for the evaluation of gas-phase viscosities, conductivities, and diffusion coefficients. *Sandia Rep.* SAND83-8209.

KIM, J. S. & WILLIAMS, F. A. 1994 Contributions of strained diffusion flames to acoustic pressure response. *Combust. Flame* **98**, 279–299.

LAW, C. K. 1988 Dynamics of stretched flames. *Twenty-Second Symp. (Intl) on Combustion*, pp. 1381–1402. The Combustion Institute.

LIBBY, P. A. & WILLIAMS, F. A. 1982 Structure of laminar flamelets in premixed turbulent combustion. *Combust. Flame* **44**, 287–303.

LIBBY, P. A. & WILLIAMS, F. A. 1984 Stretched premixed laminar flames with two reaction zones. *Combust. Sci. Tech.* **37**, 221–252.

LINAN, A. & CRESPO, A. 1976 An asymptotic analysis of unsteady diffusion flames for large activation energies. *Combust. Sci. Tech.* **14**, 95–117.

MCINTOSH, A. C., BATLEY, G. & BRINDLEY J. 1993 Short length scale pressure pulse interactions with premixed flames. *Combust. Sci. Tech.* **91**, 1–13.

MILLER, J. A., KEE, R. J., SMOOKE, M. D. & GRCAR, J. F. 1984 The computation of the structure and extinction limit of a methane–air stagnation point diffusion flame. *Spring Meeting of the Western States Section of The Combustion Institute, Paper* WSS/CI 84-10.

PETERS, N. 1984 Laminar diffusion flamelet models in non-premixed turbulent combustion. *Prog. Energy Combust. Sci.* **10**, 221–252.

PETERS, N. 1986 Laminar flamelet concepts in turbulent combustion. *Twenty-First Symp. (Intl) on Combustion*, pp. 1231–1250. The Combustion Institute.

ROGG, B. 1989 Numerical analysis of strained premixed CH_4–air flames with detailed chemistry. In *Numerical and Applied Mathematics* (ed. W. F. Ames.), pp. 159–167. J. C. Baltzer AG.

RUTLAND, C. J. & FERZIGER, J. H. 1990 Unsteady strained premixed laminar flames. *Combust. Sci. Tech.* **73**, 305–326.

SAITOH, T. & OTSUKA, Y. 1976 Unsteady behavior of diffusion flames and premixed flames for counter flow geometry. *Combust. Sci. Tech.* **12**, 135–146.

SMOOKE, M. D., PURI, I. K. & SESHADRI, K. 1986 A comparison between numerical and experimental measurements of the structure of a counterflow diffusion flame burning diluted methane in diluted air. *Twenty-First Symp. (Intl) on Combustion*, pp. 1783–1792. The Combustion Institute.

SPALDING, D. B. 1978 Counterflow Diffusion Flames. *Seventeenth Symp. (Intl) on Combustion*, pp. 431–440. The Combustion Institute.

STAHL, G. & WARNATZ, J. 1991 Numerical investigation of time-dependent properties and extinction of strained methane– and propane–air flamelets. *Combust. Flame* **85**, 285–299.

STRAHLE, W. C. 1965 Periodic solutions to a convective droplet burning problem: the stagnation point. *Tenth Symp. (Intl) on Combustion*, pp. 1315–1325. The Combustion Institute.

WHITE, F. M. 1991 *Viscous Fluid Flow*, *2nd* edn. McGraw-Hill.

WILLIAMS, F. A. 1985 *Combustion Theory*, *2nd* edn. Benjamin/Cummings.

WU, C. K. & LAW, C. K. 1984 On the determination of laminar flame speeds from stretched flames. *Twentieth Symp. (Intl) on Combustion*, pp. 1941–1949. The Combustion Institute.

YU, G., LAW, C. K. & WU, C. K. 1986 Laminar flame speeds of hydrocarbon + air mixtures with hydrogen addition. *Combust. Flame* **63**, 339–347.

ZHU, D. L., EGOLFOPOULOS, F. N. & LAW, C. K. 1988 Experimental and numerical determination of laminar flame speeds of methane/(Ar, N_2, CO_2)–air mixtures as function of stoichiometry, pressure, and flame temperature. *Twenty-Second Symp. (Intl) on Combustion*, pp. 1537–1545. The Combustion Institute.